The Electron Canonical Battery Effect in Magnetic Reconnection: Completion of the Electron Canonical Vorticity Framework

Young Dae Yoon and Paul M. Bellan[1]
Department of Applied Physics and Materials Science, Caltech, Pasadena, CA 91125

A widespread practice in studying magnetic reconnection is to examine the electron momentum equation. Here we present an alternative, *ab initio* framework that examines the motion of the electron canonical vorticity, which is the curl of the electron canonical momentum. The competition between just two terms — the convective term and the electron canonical battery term — determines the dynamics of electron canonical vorticity and equivalently the electron physics down to first principles. To demonstrate the power of this approach, the growth, saturation, stability, and morphology of the electron diffusion region are explained within the electron canonical vorticity framework. The framework provides a clear distinction between reconnection models where the frozen-in property of the magnetic field is violated by electron inertia and by pressure tensor effects such as electron viscosity, respectively.

Canonical vorticity, the curl of canonical momentum, is an important quantity in plasma physics since each species' canonical vorticity is frozen into its fluid to the extent that non-ideal phenomena such as collisions can be ignored. This freezing-in of canonical vorticity is analogous to the freezing-in of magnetic flux in ideal magnetohydrodynamics (MHD), but frozen-in canonical vorticity is more fundamental than a fluid property as it is valid in kinetic regimes with proper generalizations[1]. By generalizing familiar ideas like frozen-in flux from ideal MHD, the usage of canonical vorticity allows for physical, intuitive explanations of complicated phenomena such as magnetic reconnection — the process where magnetic field changes topology to release its energy[2].

As shown in Fig. 1, a typical collisionless reconnection geometry involves two different shear length scales $L = B/|\nabla B|$ for the magnetic field $\mathbf{B}(\mathbf{x}, t)$. The initial opposing magnetic field lines shown as black in Fig. 1 reconnect in the electron diffusion region (EDR; tan box). In the EDR the magnetic field shear length scales as $L \sim d_e$ where $d_e = c/\omega_{pe}$ is the electron skin depth. In contrast, ions diffuse within a broader region (green box) having characteristic shear scale $L \sim d_i$ where $d_i = c/\omega_{pi}$ is the ion skin depth. This difference in ion and electron flow generates quadrupole out-of-plane Hall magnetic fields (plus and minus signs). The inset shows the set of coordinates that will be used throughout this paper: x is the direction of the reconnected field and the electron inflow, y is the direction of the initial sheared magnetic field and the electron outflow, and z is the out-of-plane direction.

It has been previously demonstrated that the convection of electron canonical vorticity with the electron flow is responsible for the growth of the reconnection instability at electron scales[3–8]. This demonstration provided the intuitive interpretation that the out-of-plane electron flow stretches and thins a typical canonical vorticity flux tube in three dimensions, resulting in a purely growing instability that accelerates electrons[7,8].

The purpose of this paper is to demonstrate that an effect which we define as the "electron canonical battery" completes the electron canonical vorticity framework for magnetic reconnection with validity extending to the Vlasov frame of reference. In contrast to the generalized Ohm's law where multiple terms must be considered, the generalized canonical induction equation comprises just two terms, the convective term and the canonical battery term. The description of reconnection phenomena becomes simple because competition between these two terms determines virtually all aspects of the reconnection electron physics including growth, saturation, stability, and morphology.

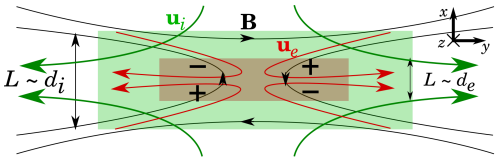

FIG. 1. A typical collisionless magnetic reconnection geometry for a zero initial out-of-plane magnetic field.

The EDR structure during reconnection has long been a subject of controversy. It was initially presumed that stable electron-scale current layers could not exist because various instabilities would break up these layers[9–11]. However, spacecraft observations showed that, in fact, the EDR has a highly elongated stable structure[12]. The stability of this elongated structure was interpreted via numerical simulations as resulting from the divergence of the pressure tensor[12–14]. However, this interpretation assumed a zero initial out-of-plane $\mathbf{B}$ field (guide field) and later numerical simulations showed that a small guide field alters the structure completely[15]. Another study showed that different regimes of the EDR exist depending on a magnetization parameter[16].

It will be shown here that, in the canonical vorticity framework, these disparities are not only easily resolved but also unified. In fact, the examination of canonical vorticity dynamics is essential for an exhaustive interpretation of the physical origin of the current structure. Different kinetic effects contribute to the canonical battery term, which then competes with the convective term

to determine the progression of the electron canonical vorticity. This progression in turn determines the overall structure, evolution, and stability of the EDR. This framework provides a simpler and clearer alternative to the traditional approach where each of the multitude of terms in the electron momentum equation is examined separately.

The sole assumption is that the ions are stationary, which is valid for $L < d_i$ corresponding to the green box in Fig. 1. While the theory to be presented is similar in many respects to classical electron-magnetohydrodynamics (EMHD)[17], the minimal restriction of this stationary-ion assumption causes the theory to differ substantively from EHMD because the assumption permits finite displacement current and the full electron pressure tensor $\mathbf{p}_e = m_e \int \mathbf{v}'_e \mathbf{v}'_e f(\mathbf{v}_e)\, d^3\mathbf{v}_e$ where $\mathbf{v}'_e$ is the random part of $\mathbf{v}_e$. In order to make the relevant equations dimensionless, quantities are normalized as follows: $\mathbf{B}$ to the upstream field strength B_0, length to d_e, time to $|\omega_{ce}|^{-1}$, $\mathbf{p}_e$ to B_0^2/μ_0, density n_e to the upstream density n_0, and $\mathbf{E}$ to $v_{Ae}B_0 = d_e\,|\omega_{ce}|\,B_0$. The dimensionless electron equation of motion is then

$$\mathbf{E} + \mathbf{u}_e \times \mathbf{B} = -\frac{D\mathbf{u}_e}{Dt} - \frac{\nabla\cdot\mathbf{p}_e}{n_e}, \tag{1}$$

where $\mathbf{u}_e$ is the electron fluid velocity. Unless specified otherwise, only normalized quantities and dimensionless equations will be used throughout this paper.

After decomposing the total derivative $D\mathbf{u}_e/Dt = \partial\mathbf{u}_e/\partial t + \mathbf{u}_e\cdot\nabla\mathbf{u}_e = \partial\mathbf{u}_e/\partial t + \nabla\left(u_e^2/2\right) - \mathbf{u}_e\times\nabla\times\mathbf{u}_e$ and defining the electron canonical vorticity

$$\mathbf{Q}_e = \nabla\times\mathbf{u}_e - \mathbf{B} = \mathbf{w}_e - \mathbf{B}, \tag{2}$$

where $\mathbf{w}_e = \nabla\times\mathbf{u}_e$ is the electron fluid vorticity, Eq. 1 can be expressed as

$$\mathbf{E} = \mathbf{u}_e\times\mathbf{Q}_e - \frac{\partial\mathbf{u}_e}{\partial t} - \nabla\left(\frac{u_e^2}{2}\right) - \frac{\nabla\cdot\mathbf{p}_e}{n_e}. \tag{3}$$

Taking the curl of Eq. 3 and using Faraday's law $\nabla\times\mathbf{E} = -\partial\mathbf{B}/\partial t$ yields the generalized canonical induction equation

$$\frac{\partial\mathbf{Q}_e}{\partial t} = \nabla\times(\mathbf{u}_e\times\mathbf{Q}_e) - \nabla\times\left(\frac{\nabla\cdot\mathbf{p}_e}{n_e}\right). \tag{4}$$

An important property of $\mathbf{Q}_e$ is that since $\mathbf{w}_e = \nabla\times\mathbf{u}_e \sim \nabla\times(\nabla\times\mathbf{B}) \sim \mathbf{B}/L^2$ where $L = B/|\nabla B|$, Eq. 2 shows that $\mathbf{Q}_e \sim \mathbf{B}/L^2 - \mathbf{B} \simeq -\mathbf{B}$ for $L \gg 1$ whereas $\mathbf{Q}_e \simeq \mathbf{w}_e$ for $L \ll 1$. For regions where $L \sim 1$ such as the EDR, both $\mathbf{w}_e$ and $\mathbf{B}$ are important. In dimensioned quantities, $e\mathbf{Q}_e = \nabla\times\mathbf{P}_e$ where $\mathbf{P}_e = m_e\mathbf{u}_e + q_e\mathbf{A}$ is the electron canonical momentum. It should be noted that Eq. 4 is also valid for any plasma species given a proper normalization.

The electron canonical vorticity dynamics governing electron physics is thus reduced to just the two terms on the right hand side of Eq. 4. The $\nabla\times(\mathbf{u}_e\times\mathbf{Q}_e)$ term is a convective term which prescribes that $\mathbf{Q}_e$ flux is frozen into $\mathbf{u}_e$, and thus provides an intuitive understanding of the temporal development of $\mathbf{Q}_e$. This convective term is responsible for the zero-beta electron physics of the reconnection instability[3–8]. By itself, this convective term causes but cannot terminate the growth of this instability. This is seen by examining the y-component of Eq. 4 near the $x = 0$ line with only the convective term retained, i.e.,

$$\frac{DQ_{ey}}{Dt} = \mathbf{Q}_e\cdot\nabla u_{ey} - Q_{ey}\left(\nabla\cdot\mathbf{u}_e\right) = -Q_{ey}\frac{\partial u_{ex}}{\partial x}. \tag{5}$$

Here we have used $\nabla\cdot\mathbf{Q}_e = 0$ from Eq. 2 and also $Q_{ex} = 0$ because $\mathbf{Q}_e$ cannot reconnect if only the convective term is retained (recall that finite Q_{ex} corresponds to reconnection of $\mathbf{Q}_e$). Since in the vicinity of the reconnection region the electron inflow has the dependence $u_{ex} \sim -x$, the quantity $-\partial u_{ex}/\partial x$ is strictly positive, so Eq. 5 produces a solution for Q_{ey} that grows exponentially in time.

Since the convective term describes freezing-in of the vorticity flux to the flow, $-\nabla\times(\nabla\cdot\mathbf{p}_e/n_e)$ is the only term in Eq. 4 that enables diffusion of $\mathbf{Q}_e$ across $\mathbf{u}_e$ or vice-versa. This term will be called the "electron canonical battery" term because in the limit of isotropic pressure (i.e. $\mathbf{p}_e = p_e\mathbf{I} = n_eT_e\mathbf{I}$), $-\nabla\times(\nabla p_e/n_e) = (\nabla n_e\times\nabla T_e)/n_e$ is the Biermann battery term[18], and because $-\nabla\times(\nabla\cdot\mathbf{p}_e/n_e)$ generates $\mathbf{Q}_e$ as indicated by Eq. 4. Since Eq. 1 results from the collisionless Vlasov equation without approximations, Eq. 4 is kinetically exact.

In order to illustrate how the competition between the convective term and the canonical battery term governs magnetic reconnection, we have developed a numerical simulation that includes compressibility, displacement current, and kinetic effects. This simulation solves the normalized Faraday's Law, Ampère's law, electron continuity equation, and generalized Ohm's law (i.e., Eq. 1) in terms of $\mathbf{j} = -n_e\mathbf{u}_e$. These equations are

$$\begin{aligned}
\frac{\partial\mathbf{B}}{\partial t} &= -\nabla\times\mathbf{E},\\
\frac{\partial\mathbf{E}}{\partial t} &= \frac{\omega_{pe}^2}{\omega_{ce}^2}\left(\nabla\times\mathbf{B} - \mathbf{j}\right),\\
\frac{\partial n_e}{\partial t} &= \nabla\cdot\mathbf{j},\\
\frac{\partial\mathbf{j}}{\partial t} &= n_e\mathbf{E} - \mathbf{j}\times\mathbf{B} + \nabla\cdot\left(\frac{\mathbf{jj}}{n_e}\right) + \nabla\cdot\mathbf{p}_e.
\end{aligned} \tag{6}$$

The set of Eqs. 6 solves Eq. 4 exactly and includes finite displacement current. The numerical method is a finite-difference-time-domain (FDTD) scheme with a semi-implicit treatment of $\mathbf{j}$, and periodic boundary conditions are used.

Two different kinetic effects are considered, namely pressure anisotropy and electron viscosity. Pressure anisotropy is modeled using the following closure which

is described in Egedal *et al.*[19] and Le *et al.*[20]:

$$\tilde{p}_{e\parallel} = \tilde{n}_e \frac{2}{2+\alpha} + \frac{\pi \tilde{n}_e^3}{6\tilde{B}^2}\frac{2\alpha}{2\alpha+1}, \tag{7}$$

$$\tilde{p}_{e\perp} = \tilde{n}_e \frac{1}{1+\alpha} + \tilde{n}_e \tilde{B}\frac{\alpha}{\alpha+1}. \tag{8}$$

In Eqs. 7 and 8 the tilde represents normalization to far upstream values (e.g., $\tilde{n}_e = n_e/n_0$) and the parameter $\alpha = \tilde{n}_e^3/\tilde{B}^2$ acts as a switch between having an isothermal (small α) or a double adiabatic (large α) equation of state. Equations 7 and 8 are approximations of second order moments of an electron distribution function derived from an analysis of electron trapping by a combination of parallel electric fields and magnetic mirrors. The situation where $\alpha \gg 1$ represents trapped electrons because magnetic mirrors trap electrons at regions of low $\mathbf{B}$ and these trapped electrons increase the local electron density. The trapped electrons conserve their first and second adiabatic invariants and thus obey Chew-Goldberg-Low[21] closure. On the other hand, $\alpha \ll 1$ represents untrapped electrons that provide an isothermal closure. This closure given by Eqs. 7 and 8, valid in the regime $v_{Te} \gg v_A$, enables fluid models to exhibit kinetic effects missing from an isotropic pressure closure by allowing for pressure anisotropy to have both spatial and temporal dependence as given by the local instantaneous value of α[22].

Equations 7 and 8 contribute to the pressure tensor as $\mathbf{p}_{e,aniso} = p_{e\perp}\mathbf{I} + \sigma\mathbf{BB}$,where $\sigma = \left(p_{e\parallel} - p_{e\perp}\right)/B^2$. The effect of electron viscosity is expressed as $\mathbf{p}_{e,vis} = -\mu\nabla\mathbf{u}_e$, where μ is the dynamic viscosity. Because conventional viscosity is in many cases negligible, μ represents an effective viscosity that includes, for example, turbulent viscosity[23] and/or hyper-resistivity[24]. The total pressure tensor is then the sum of the partial pressures; i.e., $\mathbf{p}_e = \mathbf{p}_{e,aniso} + \mathbf{p}_{e,vis}$.

The simulation was initiated by imposing a magnetic perturbation on a periodic force-free equilibrium used in Drake[25] and Ohia *et al.*[22], given by

$$B_y \simeq \tanh\left(\frac{x}{\lambda}\right) - \tanh\left(\frac{x - x_{max}/2}{\lambda}\right) - 1, \tag{9}$$

$$B_z = \sqrt{1 + B_g^2 - B_y^2\,(x)}, \tag{10}$$

where x_{max} is the size of the domain, B_g is the out-of-plane field far from the reconnection region, and λ is the half-thickness of the shear and $\lambda \ll x_{max}$. Equation 10 characterizes a guide field that renders $B^2 = B_y^2 + B_z^2$ uniform everywhere. Uniform initial pressure and density are also imposed, so the equilibrium system is initially force-free. The system is solved in 2D where $\partial/\partial z = 0$, and the grid size is 512×1024 with 25 grid points per d_e in the x direction and 10 per d_e in the y direction. Fixed parameters are $\omega_{ce}/\omega_{pe} = 1/2$, $B_g = 0.4$, and $\lambda = 2$. This extremely thin current sheet not only models the small scale of the EDR, but is also highly relevant in space plasma phenomena such as electron-only reconnection in the turbulent magnetosheath[26].

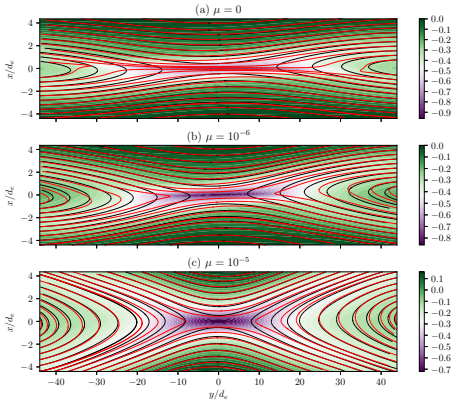

FIG. 2. In-plane $\mathbf{Q}_e$ (red), in-plane $\mathbf{B}$ (black) and u_{ez} (color) for varying μ values and isotropic pressure at $t =$ (a) 380, (b) 450, (c) 560.

In order to verify the results from the fluid simulation, the particle-in-cell (PIC) code SMILEI[27] was used to simulate reconnection with the same parameters as the fluid simulation. The realistic ion to electron mass ratio, $m_i/m_e = 1836$, was used with $\sim 2 \times 10^8$ ions and the same number of electrons. The results from the fluid simulation are mainly presented because of the ability to include, exclude, or control particular physics, and because of the clarity of presentation.

We first examine how electron viscosity affects the evolution of $\mathbf{Q}_e$. Electron viscosity contributes to the canonical battery term as $-\nabla \times \left(n_e^{-1}\nabla \cdot [-\mu\nabla\mathbf{u}_e]\right) = \nabla \times \left(\mu n_e^{-1}\nabla^2\mathbf{u}_e\right) \simeq \mu n_e^{-1}\nabla^2\mathbf{w}_e$. If $L \ll 1$ so that $\mathbf{Q}_e \simeq \mathbf{w}_e$ and thus $\nabla^2\mathbf{w}_e \simeq \nabla^2\mathbf{Q}_e$, Eq. 4 becomes

$$\frac{\partial \mathbf{Q}_e}{\partial t} = \nabla \times (\mathbf{u}_e \times \mathbf{Q}_e) + \frac{\mu}{n_e}\nabla^2\mathbf{Q}_e, \tag{11}$$

which has the same form as the resistive-MHD induction equation, $\partial\mathbf{B}/\partial t = \nabla \times (\mathbf{U} \times \mathbf{B}) + (\eta/\mu_0)\,\nabla^2\mathbf{B}$. Thus at electron scales, electron viscosity allows $\mathbf{Q}_e$ to reconnect, similar to how resisitivity allows $\mathbf{B}$ to reconnect. To mitigate confusion, we emphasize that all fluid simulations presented here solve the set of Eqs. 6, not reduced equations such as Eq. 11.

Figure 2 shows, for three different values of viscosity, the out-of-plane electron flow u_{ez} (color), in-plane $\mathbf{B}$ (black lines), and in-plane $\mathbf{Q}_e$ (red lines) for a situation with isotropic pressure (initially $\beta_e = 0.3$). Different times are chosen for each viscosity value because viscosity changes how much time is required for the EDR to display its characteristic structure. For $\mu = 0$ (Fig. 2a) the system is ideal, so $\mathbf{Q}_e$ lines remain connected and pile up near the $x = 0$ line in contrast to $\mathbf{B}$ lines which reconnect[4,5,7,8]. For finite μ (Figs. 2b and 2c), $\mathbf{Q}_e$ lines

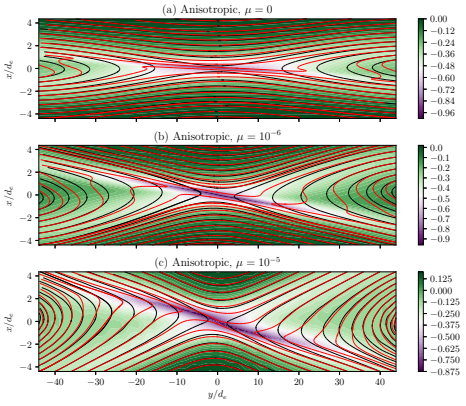

FIG. 3. Same as Fig. 2 with pressure anisotropy and varying μ values at $t =$ (a) 400, (b) 500, (c) 630.

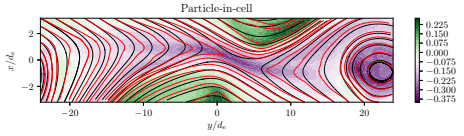

FIG. 4. Same as Fig. 2 from the particle-in-cell simulation at $t = 300$.

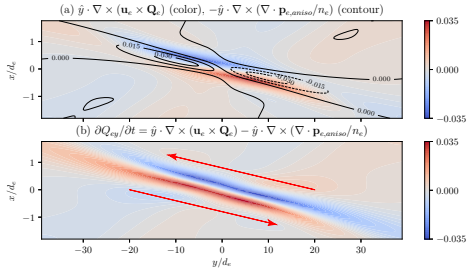

FIG. 5. (a) The y-component of the convective term $\hat{y}\cdot\nabla\times(\mathbf{u}_e\times\mathbf{Q}_e)$ (color) and the anisotropic contribution to the canonical battery term $-\hat{y}\cdot\nabla\times(\nabla\cdot\mathbf{p}_{e,aniso}/n_e)$ (contour) for the simulation corresponding to Fig. 3b. (b) The sum of $\hat{y}\cdot\nabla\times(\mathbf{u}_e\times\mathbf{Q}_e)$ and $-\hat{y}\cdot\nabla\times(\nabla\cdot\mathbf{p}_{e,aniso}/n_e)$, which is equal to $\partial Q_{ey}/\partial t$. The red arrows represent the direction of $\mathbf{Q}_e$.

reconnect as well. It is apparent from Fig. 2 that the out-of-plane electron current structure (i.e., color contours) is well manifested by in-plane $\mathbf{Q}_e$ but not by $\mathbf{B}$ — a feature that is an important advantage of using $\mathbf{Q}_e$ over $\mathbf{B}$ at electron scales. Fine structures (i.e. small L) of $\mathbf{u}_e$ are not manifested by $\mathbf{B}$ because $|\mathbf{B}| \sim |\mathbf{j}|\, L \sim |\mathbf{u}_e|\, L$ by Ampére's law, whereas they are well manifested by $\mathbf{Q}_e$ because $|\mathbf{Q}_e| \sim |\mathbf{u}_e|\,/L$.

Another important feature is that the local increase of Q_{ey} shear corresponds to the local increase of u_{ez}. To illustrate this point we consider the implications of an assumed hypothetical toy scenario where $Q_{ey} \sim A\,(t)\, x \exp\left(-x^2\right)$ where $A\,(t)$ increases in time. This profile represents locally sheared Q_{ey}. Using $u_{ez} = -\int w_{ey} dx \simeq -\int Q_{ey} dx$ for $L \ll 1$ gives $u_{ez} \sim A\,(t) \exp\left(-x^2\right)$, corresponding to a local increase in u_{ez}.

We next examine how pressure anisotropy affects $\mathbf{Q}_e$. In order to bring the system to an anisotropy-driven state faster, an initial pressure anisotropy with $\beta_{e\parallel} = 0.6$ and $\beta_{e\perp} = 0.1$ was imposed. The results for different μ are shown in Figs. 3a-c. In comparison to the isotropic case it is seen that pressure anisotropy greatly distorts the in-plane $\mathbf{Q}_e$ lines so that they pile up in the upper-left and lower-right quadrants; this corresponds to the anisotropic regime in Ohia *et al.*[22]. Again, the out-of-plane current structure is correlated with $\mathbf{Q}_e$ rather than with $\mathbf{B}$; u_{ez} is enhanced at locations where Q_{ey} is sheared. The distortion of $\mathbf{Q}_e$ field lines and the corresponding elongation and tilt of the out-of-plane current are reproduced by the PIC simulation, as shown in Fig. 4.

The anisotropic contribution to the electron canonical battery term explains the origin of the distortion of $\mathbf{Q}_e$ and equivalently the origin of the elongation of u_{ez}. Figure 5a shows the convective term $\hat{y}\cdot\nabla\times(\mathbf{u}_e\times\mathbf{Q}_e)$ (color) and the battery term $-\hat{y}\cdot\nabla\times(\nabla\cdot\mathbf{p}_{e,aniso}/n_e)$ (contour). The derivation of why $-\hat{y}\cdot\nabla\times(\nabla\cdot\mathbf{p}_{e,aniso}/n_e)$ exhibits such a structure is explained in detail in the Supplementary Material. Figure 5b shows the sum of the two terms which is equal to $\partial Q_{ey}/\partial t$, and the red arrows show the direction of Q_{ey}. It can be seen that $-\hat{y}\cdot\nabla\times(\nabla\cdot\mathbf{p}_{e,aniso}/n_e)$ adds to $\hat{y}\cdot\nabla\times(\mathbf{u}_e\times\mathbf{Q}_e)$ and increases the spatial extent of $\partial Q_{ey}/\partial t$; this in turn elongates the structure of u_{ez}.

The examination of $\mathbf{Q}_e$ dynamics and the electron canonical battery term is not only advantageous but in fact essential for the correct interpretation of a given EDR structure. For example, Ohia *et al.*[22] observed that imposing isotropic pressure deformed the out-of-plane current structure to be less elongated, which seemingly contradicts Fig. 2a. However, in Ohia *et al.*[22], an effective electron viscosity of 1.5×10^{-5} with the same normalized units as this study was imposed, approximately corresponding to Fig. 2c. Thus, it is not isotropic pressure that leads to an out-of-plane current localized at the origin; instead, the current localization results from the reconnection of $\mathbf{Q}_e$ by electron viscosity.

Another such example is the origin of elongated EDR structures. The elongated structure in Fig. 2a results from the pile-up of $\mathbf{Q}_e$ field lines due to the lack of significant electron viscosity, whereas the elongated structures in Fig. 3 result from pressure anisotropy. Therefore, in order to give correct physical interpretations, the

scrutiny of the electron canonical battery term and the ensuing canonical vorticity dynamics is vital.

In Ohia *et al.*[22], it was found that the plasma approaches the firehose condition along the elongated current layer. This phenomenon can be simply explained by a direct comparison between the convective term and the electron canonical battery term. On scales $L > d_e$, the convective term goes like $\nabla \times (\mathbf{u}_e \times \mathbf{Q}_e) \simeq \nabla \times (\mathbf{u}_e \times \mathbf{B}) \simeq -\nabla \times ([\nabla \times \mathbf{B}] \times \mathbf{B}) \sim B^2/L^2$, and the anisotropic contribution to the canonical battery term goes like $\nabla \times (\nabla \cdot [\sigma \mathbf{B}\mathbf{B}]) \sim \sigma B^2/L^2$. It follows that $\sigma \sim 1$ or $\left(p_{e\parallel} - p_{e\perp}\right)/B^2 \sim 1$ in order for the two terms to be commensurate; thus, the parallel and perpendicular electron pressures approach the firehose criterion.

Equation 11 stipulates the condition for the instability of the EDR. Because $\mathbf{Q}_e \simeq \mathbf{w}_e$ for $L \ll 1$, Eq. 11 is equivalent to the electron fluid vorticity equation $\partial \mathbf{w}_e/\partial t = \nabla \times (\mathbf{u}_e \times \mathbf{w}_e) + (\mu/n_e)\nabla^2 \mathbf{w}_e$. It then naturally follows from fluid dynamics that turbulent flow develops at a sufficiently high Reynolds number $Re \sim n_e/\mu$. This unstable regime corresponds to the regimes in Drake *et al.*[10] and Del Sarto *et al.*[11].

Equation 4 clarifies the distinction between a tearing-mode-type reconnection instability and a Sweet-Parker-type quasi-steady-state reconnection. By itself the convective term yields an exponentially growing solution even in the non-linear regime, as shown by Eq. 5. Thus, if the canonical battery term is not sufficiently large to be significant in Eq. 4, a quasi-steady-state reconnection or reconnection saturation cannot be achieved.

Equation 4 also clarifies the distinction between reconnection models where the magnetic field is broken only by electron inertia[5] and those where it is broken also by pressure tensor effects such as electron viscosity[28,29]. If only the electron inertia term is included, then the system is entirely described by the convective term in Eq. 4, whereas the electron viscosity is manifested by the electron canonical battery term. A possible scenario is that electron inertia breaks the magnetic fields during earlier times, but the EDR is subject to instabilities and turbulence due to the high Reynolds number at latter times. These instabilities increase the effective viscosity, which makes the canonical battery term break both the magnetic field and the canonical vorticity field. Whether a particular reconnection event is affected by mostly the convective term or by both the convective term and the canonical battery term depends on the parameters and the time-scale of the system.

The advantage of the canonical vorticity framework is now clear. The convective term in Eq. 4 signifies the convection of $\mathbf{Q}_e$ with $\mathbf{u}_e$, which intuitively explains reconnection electron physics for zero beta (no pressure). One can then study how a particular kinetic effect, such as electron presssure anisotropy, viscosity, or distribution function foliation[30], influences reconnection by examining how that effect is manifested in the canonical battery term and then competes with the convective term. This is not only much simpler than examining multiple terms in the generalized Ohm's law, but also exhaustive because Eq. 4 is a direct consequence of the collisionless Vlasov equation.

In summary, the electron canonical battery term completes the canonical vorticity framework of the electron physics in magnetic reconnection. As demonstration of the power of this approach, the growth, saturation, stability, and morphology of the EDR have been reinterpreted, expanded, and unified within this framework. In particular, the framework illustrates how the changes in the electron fluid closure (Eqs. 7 and 8) affect the current structure through the electron canonical battery term. The distinction between electron-inertia-driven and pressure-tensor-driven models of reconnection is also clearly demonstrated. The simple yet complete nature of this framework makes it an appealing alternative to the traditional magnetic-field-based approach to magnetic reconnection.

SUPPLEMENTARY MATERIAL

See supplementary material for the derivation of how different terms compete to yield the structure of the electron canonical battery shown in Fig. 5a (contour).

ACKNOWLEDGMENTS

This material is based upon work supported by the U.S. Department of Energy Office of Science, Office of Fusion Energy Sciences under award No. DE-FG02-04ER54755 and by the Air Force Office of Scientific Research under award No. FA9550-17-1-0023. The computations presented here were conducted on the Caltech High Performance Cluster, partially supported by a grant from the Gordon and Betty Moore Foundation.

[1] S. You, Physics of Plasmas **23**, 072108 (2016), arXiv:1607.00551.
[2] M. Yamada, R. Kulsrud, and H. Ji, Reviews of Modern Physics **82**, 603 (2010), arXiv:arXiv:0708.1752.
[3] M. Ottaviani and F. Porcelli, Physical Review Letters **71**, 3802 (1993).
[4] D. Biskamp, E. Schwarz, and J. F. Drake, Physics of Plasmas **4**, 1002 (1997).
[5] E. Cafaro, D. Grasso, F. Pegoraro, F. Porcelli, and A. Saluzzi, Physical Review Letters **80**, 4430 (1998).
[6] D. Grasso, F. Califano, F. Pegoraro, and F. Porcelli, Physical Review Letters **86**, 5051 (2001).
[7] Y. D. Yoon and P. M. Bellan, Physics of Plasmas **24** (2017), 10.1063/1.4982812.
[8] Y. D. Yoon and P. M. Bellan, Physics of Plasmas **25** (2018), 10.1063/1.5016345.
[9] J. F. Drake, R. G. Kleva, and M. E. Mandt, Physical Review Letters **73**, 1251 (1994).
[10] J. F. Drake, D. Biskamp, and A. Zeiler, Journal of Geophysical Research: Space Physics **24**, 2921 (1997).
[11] D. Del Sarto, F. Califano, and F. Pegoraro, Physical Review Letters **91**, 2350011 (2003).
[12] T. D. Phan, J. F. Drake, M. A. Shay, F. S. Mozer, and J. P. Eastwood, Physical Review Letters **99**, 255002 (2007).

[13]H. Karimabadi, W. Daughton, and J. Scudder, Geophysical Research Letters **34**, n/a (2007).
[14]M. A. Shay, J. F. Drake, and M. Swisdak, Physical Review Letters **99**, 155002 (2007), arXiv:0704.0818.
[15]M. V. Goldman, G. Lapenta, D. L. Newman, S. Markidis, and H. Che, Physical Review Letters **107**, 135001 (2011), arXiv:1011.0103.
[16]A. Le, J. Egedal, O. Ohia, W. Daughton, H. Karimabadi, and V. S. Lukin, Physical Review Letters **110**, 135004 (2013).
[17]S. V. Bulanov, F. Pegoraro, and A. S. Sakharov, Physics of Fluids B: Plasma Physics **4**, 2499 (1992).
[18]L. Biermann, Zeitschrift Naturforschung Teil A **5**, 65 (1950).
[19]J. Egedal, W. Fox, N. Katz, M. Porkolab, M. Øieroset, R. P. Lin, W. Daughton, and J. F. Drake, Journal of Geophysical Research: Space Physics **113**, n/a (2008).
[20]A. Le, J. Egedal, W. Daughton, W. Fox, and N. Katz, Physical Review Letters **102**, 085001 (2009).
[21]G. F. Chew, M. L. Goldberger, and F. E. Low, Proceedings of the Royal Society of London. Series A. Mathematical and Physical Sciences **236**, 112 (1956).
[22]O. Ohia, J. Egedal, V. S. Lukin, W. Daughton, and A. Le, Physical Review Letters **109**, 115004 (2012).
[23]J. Boussinesq, Mémoires présentés par divers savants à l'Académie des Sciences **23**, 1 (1877).
[24]H. R. Strauss, Physics of Fluids **29**, 3668 (1986).
[25]J. F. Drake, Science **299**, 873 (2003).
[26]T. D. Phan, J. P. Eastwood, M. A. Shay, J. F. Drake, B. U. Sonnerup, M. Fujimoto, P. A. Cassak, M. Øieroset, J. L. Burch, R. B. Torbert, A. C. Rager, J. C. Dorelli, D. J. Gershman, C. Pollock, P. S. Pyakurel, C. C. Haggerty, Y. Khotyaintsev, B. Lavraud, Y. Saito, M. Oka, R. E. Ergun, A. Retino, O. Le Contel, M. R. Argall, B. L. Giles, T. E. Moore, F. D. Wilder, R. J. Strangeway, C. T. Russell, P. A. Lindqvist, and W. Magnes, Nature **557**, 202 (2018).
[27]J. Derouillat, A. Beck, F. Pérez, T. Vinci, M. Chiaramello, A. Grassi, M. Flé, G. Bouchard, I. Plotnikov, N. Aunai, J. Dargent, C. Riconda, and M. Grech, Computer Physics Communications **222**, 351 (2018), arXiv:arXiv:1702.05128v1.
[28]P. Ricci, J. U. Brackbill, W. Daughton, and G. Lapenta, Physics of Plasmas **11**, 4102 (2004), arXiv:0304224 [astro-ph].
[29]M. Hesse, Physics of Plasmas **13** (2006), 10.1063/1.2403784.
[30]T. V. Liseikina, F. Pegoraro, and E. Y. Echkina, Physics of Plasmas **11**, 3535 (2004).

PLEASE CITE THIS ARTICLE AS DOI: 10.1063/1.5122225